Shape Reconstruction Incorporating Multiple Non-linear Geometric Constraints

Naoufel Werghi, Robert Fisher, Craig Roberstson and Anthony Ashbrook
Division of Informatics, University of Edinburgh
5 Forrest Hill, Edinburgh EH1 2QL, UK
Email: {naoufelw, rbf, anthonya, craigr}@dai.ed.ac.uk

Abstract. This paper deals with the reconstruction of of 3D geometric shapes based on observed noisy 3D measurements and multiple coupled non-linear shape constraints. Here a shape could be a complete object, a portion of an object, a part of a building etc. The paper suggests a general incremental framework whereby constraints can be added and integrated in the model reconstruction process, resulting in an optimal trade-off between minimization of the shape fitting error and the constraint tolerances. After defining sets of main constraints for objects containing planar and quadric surfaces, the paper shows that our scheme is well behaved and the approach is valid through application on different real parts. This work is the first to give such a large framework for the integration of numerical geometric relationships in object modelling from range data. The technique is expected to have a great impact in reverse engineering applications and manufactured object modelling where the majority of parts are designed with intended feature relationships.

Keywords: Reverse engineering, Geometric constraints, constrained shape reconstruction, shape optimization

Abbreviations: CAD – Computer Aided-design; 3D – Three-Dimensional

Table of Contents

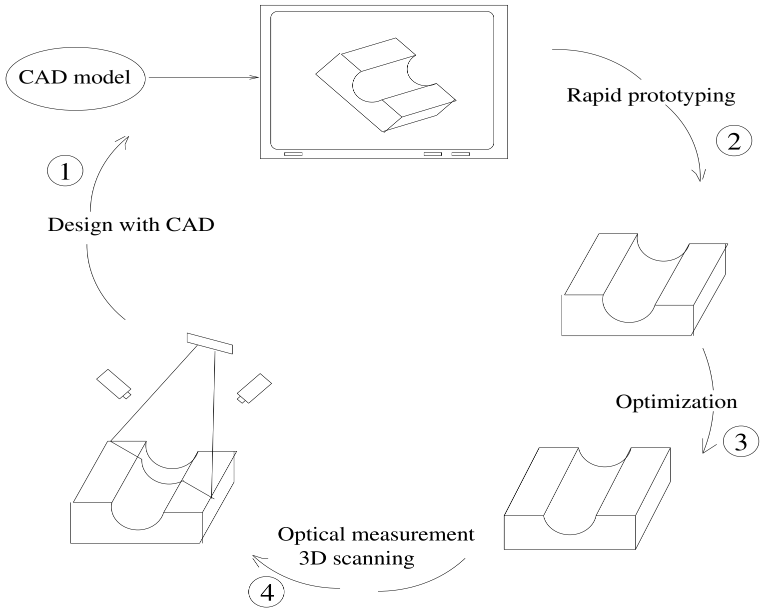

Figure 1. The production-perfection cycle of a part

1. Introduction

The framework of this work is reverse engineering. In parts manufacturing, reverse engineering is typically concerned with measuring an existing object so that a surface or solid model can be deduced in order to take advantage of CAD/CAM technologies. It is also often necessary to produce a copy of a part when no original drawings or documentation are available. In other cases we may want to re-engineer an existing part, when analysis and modifications are required to construct a new improved product. Even though it is possible to turn to a computer-aided design to fashion a new part, it is only after the real model is made and evaluated that we can see if the object fits with real world. For this reason designers rely on real 3D objects (real scale wood, clay model) as starting point. Such procedure is particularly important to areas involving aesthetic design e.g automobile industry or generation of custom fits to human surfaces such as helmets, space suits or prostheses. For these reasons reverse engineering is a fundamental step of the now-standard production-perfection cycle of part (Figure.1). This process starts with the CAD stage. Next (step 2), the rapid prototyping stage converts the CAD data into a real prototype. Rapid prototyping is a technique allowing the direct production of prototypes by a computer-controlled process. Often, the shape of the produced object undergoes some improvement carried out by hand to make it adapted to its real environment (step 3). The hand-improved model is back again into the

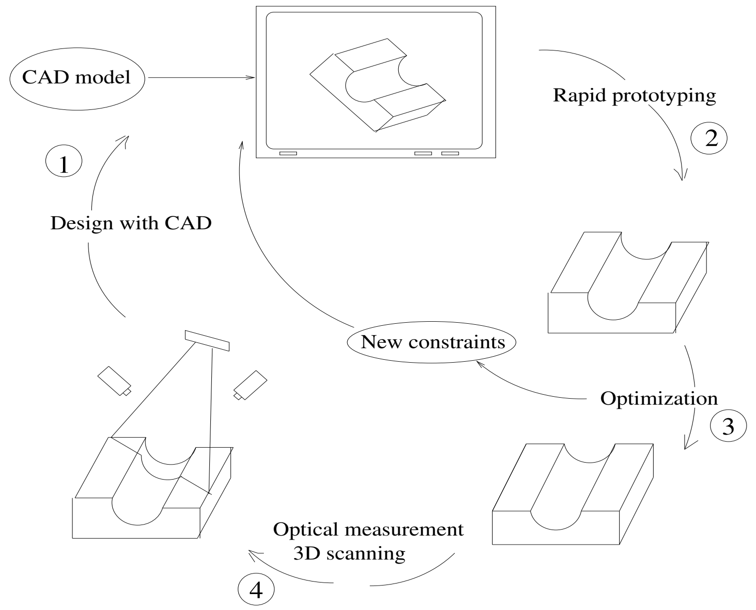

Figure 2. Many hand-worked optimization (step 3) could be replaced by establishing new constraints on the shape and incorporating them in the model design process.

digital world of CAD through 3D optical measurement techniques (step 4), in occurrence 3D laser scanner.

In this process the notion of constraints is normally involved in step 1 where geometric relationships between object features together with 3D measurement data contributes in the production of the optimal object model shape.

The first motivation behind incorporating geometric constraint is that models needed by industry are generally designed with intended geometric relationships between the object features so this aspect should be exploited rather than ignored. The consideration of these relationships is actually necessary because some attributes of the object would have no sense if the object modelling scheme did not take into account these constraints. For example, take the case when we want to estimate the distance between two parallel planes: if the plane fitting results gave two planes which are not parallel, then the distance measured between them would have no significance. Furthermore exploiting the available known relationships would be useful for reducing the effects of registration errors and mis-calibration, thus improving the accuracy of the estimated part features' parameters and consequently the quality of the modelling

The second motivation is that once the part is produced (step 2) many improvement are carried manually (step 3) to optimize the part and make it fit with the real world (e.g fit with another part, adjust the part to fit particular customer). These improvements could be represented by new constraints on the shape of the part, by integrating these constraints into the design with CAD process step (Figure.2) the work piece optimization would be reduced to the minimum tasks and hence many cycles in the part production process would be saved. In other cases, such improvement could not be achieved by hand due to the complexity of the object or when we want to extend the process for modelling buildings or plants.

A review of the main reverse engineering research in the CAD community [5, 11, 12, 15] revealed that the exploitation of geometric constraints has not been fully investigated. This lack was discussed in the survey work of Varady *et al* [13].

This work present a general framework for the incorporation of geometric constraints into the modelling process with application to reconstructing or reverse engineering objects having planar and quadric surfaces.

2. Related work

The approach for incorporating geometric relationships in object modelling has to tackle two problems, the first is how to represent the constraints? The second is how to integrate these constraints into the shape fitting process. These two aspects are not entirely independent, the shape fitting technique imposes restrictions on the constraint representation and vice versa. Besides the approach should aim for the maximum satisfaction of the constraints.

A first step in the direction of incorporating constraints for assuring the consistency of the reconstruction was done by Porrill [9]. He linearized a set of nonlinear constraints and combined them with a Kalman filter applied to wire frame model construction. Porrill's method takes advantage of the recursive linear estimation of the Kalman filter, but guarantees satisfaction of the constraints only to linearized first order. Additional iterations are needed at each step if more accuracy is required.

This last condition has been taken into account in the work of De Geeter *et al* [3] by defining a "Smoothly Constrained Kalman Filter". The key idea of their approach is to replace a nonlinear constraint by a set of linear constraints applied iteratively and updated by new measurements in order to reduce the linearization error. However, the characteristics of Kalman filtering makes these methods essentially adapted for iteratively acquired data and many data samples. Moreover, there was no mechanism for determining how successfully the constraints were satisfied and only lines and planes were considered in both of the above works.

The constraints considered by Bolle *et al* [2] in their approach to 3D object position covered only the shape of the surfaces. They chose a specific representation for the treated features: plane, cylinder and sphere.

Compared to Porrill's and De Geeter's work, our approach avoids the drawbacks of linearization, since the constraints are completely implemented. Moreover, our approach covers a larger category of feature shapes. Regarding the work of Bolle [2], the type of constraints which can be held by our approach go beyond the restricted set of surface shapes and cover also the geometric relationships between object features. To our knowledge the work appears to be the first to give such a large framework for the integration of geometric relationships for object reconstruction.

3. The Geometric constraints

The set of constraints associated with a given object can be divided mainly into two categories. The first one is the surface intrinsic constraints covering the geometric properties which arise from the specific shapes of the surfaces. This category includes particular properties of the surface such as symmetry with respect to a point or a line. For quadric surfaces such as cones or cross-section cylinders this property is the circular shape of the surface.

The second category named, the feature extrinsic constraints, defines the geometric and topological relationships between the different object features. Table I summarizes these relationships. We notice here that points and lines in this table may be either physical features of the object like summits and edges or implicit features like centres, axes of symmetry. This list is not exhaustive and this classification may not be unique. Nevertheless it covers a large number of constraints in manufactured objects.

Table I. Relationships between features.

	point	line	plane	quadric surface
point	coincident separation	inclusion separation	inclusion separation	inclusion separation
line	-	coincident relative orientation separation	inclusion relative orientation separation	inclusion relative orientation separation
plane	-	-	coincident relative orientation separation	relative orientation separation
quadric surface	-	-	-	coincident relative orientation separation

3.1. Coincidence constraints

It is common that shapes contain features which are associated to the same geometric entity (Figure.3.a) or which coincide at the same position (Figure.3.b). In the first case these constraints are implicitly imposed by considering the same parameters for each feature. In the second case the parameters associated to each feature are equated and the resulting equations have then to be satisfied.

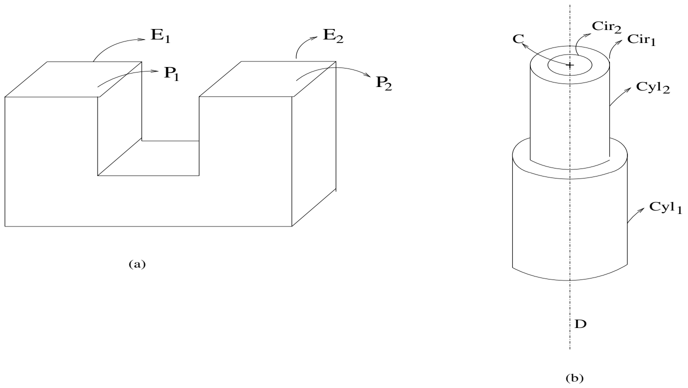

Figure 3. (a): The two edges E_1 and E_2 belong to the same line. The two faces P_1 and P_2 are associated to the same plane. (b) The centres of the circles Cir_1 and Cir_2 coincide at the same point C. The cylinders Cyl_1 and Cyl_2 have a common axis.

3.2. Inclusion constraints

A particular feature point may be included in an object feature e.g line, plane or quadric patch. Similarly a feature line may be included in a plane or a particular quadric surface (Fig.4) such as a cylinder and a cone.

3.3. Relative orientation constraint

There are many orientation relationships which can be deduced and exploited in a given part, such as the two common particular cases of parallelism and orthogonality (Fig.5.a). The presence of these two characteristics is easily detected in an object.

3.4. Relative separation constraint

The relative separation between features can be exploited when the distance between parallel features (Fig.5.b) is already known or needs to be imposed or when the object has a symmetry aspect leading to some separation distance relationships (Fig.5.c).

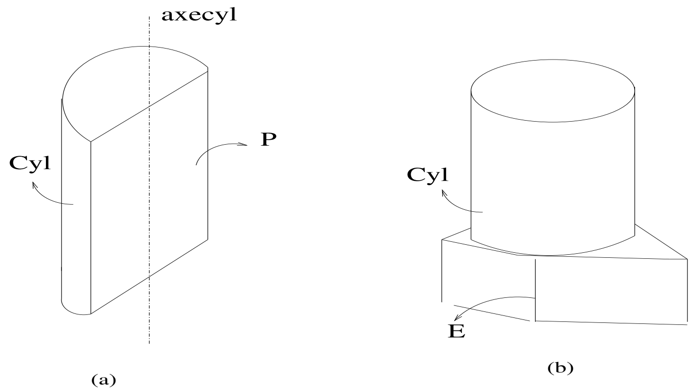

Figure 4. (a): The axis of the cylinder patch *Cyl* is included in the plane *P*. (b) The line associated to the edge *E* is included in the cylinder *Cyl*.

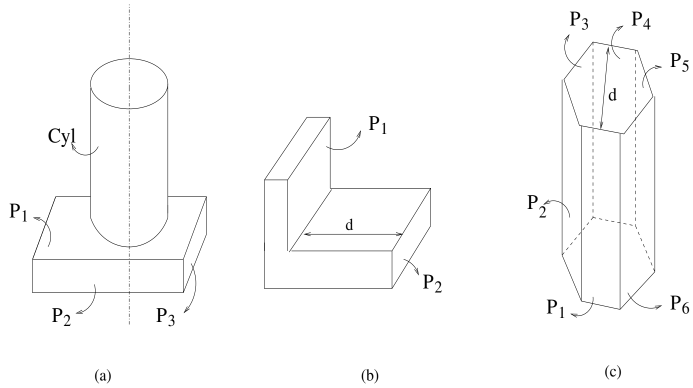

Figure 5. (a): Each pair of planes $(P_1, P2, P3)$ makes an angle of 90^o, the axis of the cylinder *Cyl* is orthogonal to P_1. (b): The planes (P_1, P_2) are separated by distance d. (c): Each pair of parallel planes of the hexagonal prism are separated by the same distance.

3.5. Other constraints

There are also other types of constraints like those imposed directly on the surface parameters as a consequence of the surface representation e.g the representation of a plane by the equation $ax + by + cz + d = 0$ where $[a, b, c]$ is normal vector to the plane and d is the distance of the plane to the origin requires that the sum of the squared elements of the normal be equal to one. Such constraints are called the unit constraints.

4. Optimization of shape satisfying the constraints

4.1. Problem definition

Given sets of 3D measurement points representing surfaces belonging to a certain shape, we want to estimate the different parameters of the surfaces, taking into account the geometric relationships between these surfaces and the specific shapes of surfaces as well.

A state vector $\vec{p}$ is associated to the object, which includes all parameters related to the patches. The shape defined by the parameter vector $\vec{p}$ has to best fit the data while satisfying the constraints. Consider $F(\vec{p})$ to be an objective function defining the relationship between the set of data and the parameters and $C_k(\vec{p})$, $k = 1..M$ the set of constraint functions defining the geometric constraints. $C_k(\vec{p})$ is a vector function associated with constraint k. The problem can be then stated as follows: Find the parameter vector $\vec{p}$ minimizing the function $F(\vec{p})$ subject to the constraints

$$C_k(\vec{p}) \leq \tau_k, \quad k = 1..M \tag{1}$$

Here τ_k represents the tolerance related to the constraint C_k. Ideally the tolerances have zero values, but practically, for geometric constraints they are assigned certain values which reflects the allowed geometric inaccuracies in the relative locations and shapes of features. It is up to the designer to set the tolerances, however an appropriate definition of the tolerances for a given object can be set up by using the scheme developed by Requicha [10].

So we are dealing with a constrained optimization problem. Optimization techniques fall into two broad branches namely classical techniques e.g Operation Research techniques and evolutionary techniques. In the proposed work we have preferred the classical techniques (a combination of Lagrange's method and Levenberg-Marquardt algorithm) firstly because they are more mature techniques and secondly because of the high computational time expense evolutionary techniques require which makes them impractical for the repetition of experiments and for verifying the results.

4.2. The optimization algorithm

According to the Lagrange technique the best parameter vector minimizing the objective function while satisfying the constraints is the one minimizing the following optimization function:

$$E(\vec{p}) = F(\vec{p}) + \sum_{k=1}^{M} \lambda_k C_k(\vec{p}) \qquad \lambda_k \geq 0 \tag{2}$$

where λ_k are weighting coefficients (known in the literature as Lagrange multipliers) used to control the contribution of the constraints in the parameters' estimation.

The method of solving this problem depends on the nature of the objective function (convex or not), the type of the constraints (linear or not) and whether the constraints could be merged together in order to reduce the number of parameters and eventually combined with the objective function.

The problem is said to be a convex optimization problem if the objective function and the constraint functions also are convex functions. Such a problem can be solved numerically with great efficiency since there is extensive and useful theory in the literature. On the other hand, the existence of an optimal solution necessitates that both the objective function and the constraint functions are differentiable. A detailed analysis of the convexity and the optimality conditions is available in [7].

Section 4.3 will show that the objective function is convex and differentiable. The constraint function has to be formulated to satisfy the above requirements.

In some particular cases it is possible to get a closed form solution for (2) (the eigenvalues methods). This depends on the characteristics of the constraint functions and whether it is possible to combine them efficiently with the objective function. Generally it is not trivial to develop a closed form solution especially when the constraints are nonlinear and their number is high. In such case an algorithmic approach could be of great help taking into account the increasing capabilities of computing. The main idea was to develop a search optimization scheme for determining the best set $(\vec{p}, \lambda_1, ., ., \lambda_k)$. Moreover, we have been investigating whether it is possible to get a solution that satisfies a specified tolerance. So the objective is to determine the vector $\vec{p}$ which satisfies the constraints to the desired specification and which fits the data to a reasonable degree.

The proposed algorithm proceeds as follows: we start with a parameter vector $\vec{p}^{[0]}$ that satisfies the least squares constraints and attempt to find a nearby vector $\vec{p}^{[1]}$ that minimizes (2) for small values λ_k, in which the constraints are weakly expressed. Then we iteratively increase the set of λ_k slightly and solve for a new optimal parameter $\vec{p}^{[n+1]}$ using the previous $\vec{p}^{[n]}$. At each iteration n, the algorithm increases each λ_k by a certain amount and a new $\vec{p}^{[n]}$ is found such that the optimization function is minimized by means of the standard Levenberg-Marquardt algorithm. The parameter vector $\vec{p}^{[n]}$ is then updated to the new estimate $\vec{p}^{[n+1]}$ which becomes the initial estimate at the next values of λ_k. The algorithm stops when the constraints are satisfied to the desired degree or when the parameter vector remains stable for a certain number of iterations.

A simplified version of the algorithm is illustrated in Figure 6 in which a single λ is associated to the constraints.

The initialization of the parameter vector is crucial to guarantee the convergence of the algorithm to the desired solution. For this reason the initial vector was the one which best fitted the set of data in the absence of con-

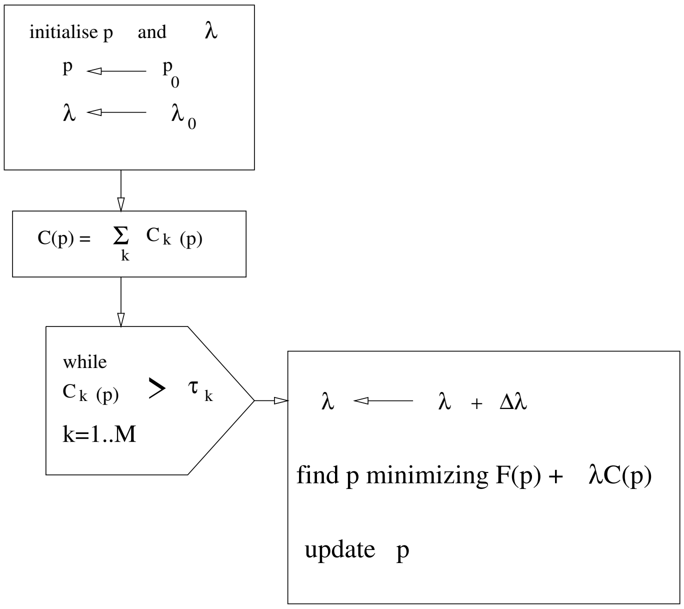

Figure 6. Optim1: the constraint optimization algorithm.

straints. This vector can be obtained by estimating each surface's parameter vector separately and then concatenating the vectors into a single one. Naturally, the option of minimizing the least objective function $F(\vec{p})$ alone has to be avoided since it leads to the trivial null vector solution. On another hand, the initial values λ_k have to be large enough to avoid the above trivial solution and to give the constraints a certain weight. A convenient value for the initial λ_k is :

$$\lambda_k^{[0]} = \frac{F(\vec{p}^{[0]})}{C_k(\vec{p}^{[0]})} \tag{3}$$

where $\vec{p}^{[0]}$ is the initial parameter estimation obtained by concatenating the unconstrained estimates.

4.3. Representation of the objective function

Consider $S_1,.,.S_N$ the set of surfaces and $\vec{p}_1,.,.\vec{p}_N$ the set of parameter vectors related to them. Each vector $\vec{p}_i$ has to minimize a given surface fit error criterion J_i associated with the surface S_i such as the least squares error criterion. The set of the parameter vectors has then to minimize the following object function:

$$J = J_1 + J_2 + ...J_N \tag{4}$$

By considering a polynomial description of the surfaces, each surface S_i can be represented by:

$$\vec{h}_i^{\,T} \vec{p}_i = 0 \tag{5}$$

where $\vec{h}_i$ is the measurement vector with each component of the form $x^\alpha y^\beta z^\gamma$ for some (α, β, γ).

The advantage of this formulation is that it leads to a compact quadric expression of the objective function because of the linearity (with respect to the parameters) of surface equation (5). Indeed, given m_i measurements, the least squares criterion related to this equation is

$$J_i = \sum_{l=1}^{m_i} (\vec{h}_i^{l\,T} \vec{p}_i)^2 = \vec{p}_i^{\,T} H_i \vec{p}_i \tag{6}$$

where $H_i = \sum_{l=1}^{m_i} (\vec{h}_i^l \vec{h}_i^{l\,T})$ represents the sample covariance matrix of the surface S_i. By concatenating all the vectors $\vec{p}_i^{\,T}$ into one vector $\vec{p} = [\vec{p}_1^{\,T}, \vec{p}_2^{\,T}, ., ., ., \vec{p}_N^{\,T}]^T$ equation (4) can be written as a function of the parameter vector $\vec{p}$ and we get the following objective function:

$$F(\vec{p}) = J = \vec{p}^T \mathcal{H} \vec{p}, \qquad \mathcal{H} = \begin{bmatrix} H_1 & (0) & . & (0) \\ (0) & H_2 & . & (0) \\ (0) & . & . & (0) \\ (0) & . & (0) & H_N \end{bmatrix} \tag{7}$$

Such a function is convex if and only if the matrix $\mathcal{H}$ is positive, which is the case. Besides, under the above form, the objective equation contains separate terms for the data and the parameters. The data matrix $\mathcal{H}$ can be thus computed off-line before the optimization.

The objective function could be taken as the likelihood of the range data given the parameters (with a negative sign since we want to minimize). The likelihood function has the advantage of accounting for the statistical aspect of the measurements. As a first step, we have chosen the least squares function. The integration of the data noise characteristics in the LS function can be done afterwards with no particular difficulty, leading to the same estimation of the likelihood function in the case of the Gaussian distribution.

4.4. Constraint formulation

The different constraints are implemented under a matrix formulation. Although the use of matrices may be computationally expensive, the matrix notation leads to a compact form and avoids expressions with many variables in particular for the second order derivatives used in the Levenberg-Marquardt algorithm. This allows a fast, automatic and easy implementation of the constraints. All the constraint equations are squared in order to ensure that the constraint functions are convex.

Some intrinsic constraints, for instance circularity of quadric surfaces could be imposed implicitly by choosing a suitable form of the surface equation. However, the implementation of the reduced form in the optimization algorithm may cause some complexity. Indeed, because of the nonlinearity of the these forms, it has not been possible to get an objective function with separated terms for the data and the parameters. Thus, the data terms could not be computed off-line. This may increase the computational cost dramatically.

5. Implementation

First, the algorithm was developed and implemented under MATLAB mainly to check the the behaviour and the convergence of the algorithm as well as the validity of the results. This version rapidly turned out to be inconvenient since a new implementation is needed to be done for each part. The next step was then to develop a program which can hold any part and automatically convert the information given by the user about the object (surfaces and constraints) into a structure (set of objective function and constraint functions) ready to be integrated into the optimization algorithm. A simple constraint language compiler was developed under C++ for this purpose. The input file is a list of statements in which the user declares the surfaces, their identifications and the files where the associated 3D measurement points are stored. Then the constraints are declared with their eventual associated values and tolerances. Figure 7 shows the structure of the input file and the language statements.

The whole package (the compiler and the optimization algorithm) have been implemented on a $200Mhz$ SUN Ultrasparc workstation. The computation time is in the range of 3-10 minutes for the different tested objects. This range is suitable for CAD work.

6. A simple example

Consider a simple polyhedral object, for instance a tetrahedron. Suppose that the tetrahedron is composed from three surfaces, $S_1, S2_2$ and S_3 (Fig.8).

Following the paradigm of Section 4.3, each surface is represented by the equation:

$$\vec{h^i_j}^T \vec{p}_i = 0\,; \quad i = 1..3$$

$$\vec{h^i_j} = [x^i_j, y^i_j, z^i_j, 1]^T; \qquad \vec{p}_i = [n^i_x, n^i_y, n^i_z, d_i]^T$$

The object is then represented by the parameter vector:

$$\vec{p} = [n^1_x, n^1_y, n^1_z, d_1, n^2_x, n^2_y, n^2_z, d_2, n^3_x, n^3_y, n^3_z, d_3]$$

```
SURFACES                              /* begin of surfaces declaration */
.
SURFACE TYPE     Identifier     data file
.
END_SURFACES                          /* end of surfaces declaration */


CONSTRAINTS                           /*begin of constraints declaration */
PARALLEL_PLANES
.
Identifier1     Identifier2
.
END_PARALLEL_PLANES
INTRINSIC_CONSTRAINTS
.
Identifier     CONSTRAINT TYPE     Tolerance
.
END_INTRINSIC_CONSTRAINTS
ORIENTATION_PLANE_PLANE
.
Identifier1     Identifier2     Angle     Tolerance
.
END_ORIENTATION_PLANE_PLANE

ORIENTATION_PLANE_QUADRIC
.
Identifier1     Identifier2     Angle     Tolerance
.
END_ORIENTATION_PLANE_QUADRIC
.
.
.
END_CONSTRAINTS                       /*end of constraints declaration */
```

Figure 7. Structure of the input file for the constraint language compiler: the upper case words are the key words of the language

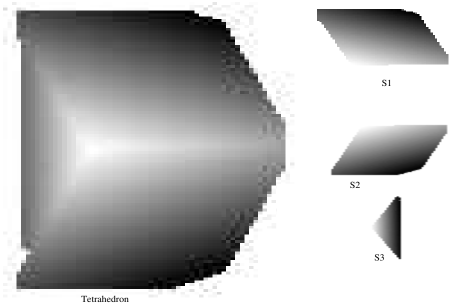

Figure 8. The tetrahedron object with the extracted surfaces

The objective function is expressed by:

$$F(\vec{p}) = J = \vec{p}^T \mathcal{H} \vec{p} = \begin{bmatrix} H_1 & (0)_4 & (0)_4 \\ (0)_4 & H_2 & (0)_4 \\ (0)_4 & (0)_4 & H_3 \end{bmatrix}$$

where

$$H_i = \sum_j (\vec{h}^i_j)(\vec{h}^i_j)^T$$

The surfaces have three orientation constraints reflecting the three angles 90^0, 90^0 and 120^0 between the three surface normals $\vec{n}_1$, $\vec{n}_2$ and $\vec{n}_3$. These constraints are represented by the following equations

$$\begin{aligned} \vec{n}_1{}^T \vec{n}_2 &= -0.5 \\ \vec{n}_1{}^T \vec{n}_3 &= 0 \\ \vec{n}_2{}^T \vec{n}_3 &= 0 \end{aligned}$$

from which the constraint functions are deduced:

$$\begin{aligned} Angle_1(\vec{p}) &= (\vec{p}^T A_1 \vec{p} + 0.5)^2 = 0 \\ Angle_2(\vec{p}) &= (\vec{p}^T A_2 \vec{p})^2 = 0 \\ Angle_3(\vec{p}) &= (\vec{p}^T A_3 \vec{p})^2 = 0 \end{aligned}$$

where

$$A_1 = \begin{cases} A_1(i,j) = A_1(j,i) = 1/2 & \text{if } i = 1+t,\ j = 5+t, \quad 0 \le t \le 2 \\ A_1(i,j) = A_1(j,i) = 0 & \text{otherwise} \end{cases}$$

$$A_2 = \begin{cases} A_2(i,j) = A_2(j,i) = 1/2 & \text{if } i = 1+t,\ j = 9+t, \quad 0 \le t \le 2 \\ A_2(i,j) = A_2(j,i) = 0 & \text{otherwise} \end{cases}$$

$$A_3 = \begin{cases} A_3(i,j) = A_3(j,i) = 1/2 & \text{if } i = 5+t,\ j = 9+t, \quad 0 \le t \le 2 \\ A_3(i,j) = A_3(j,i) = 0 & \text{otherwise} \end{cases}$$

The surfaces normals are also constrained to be unit, this leads to the following unit constraints:

$$\begin{aligned} Unit_1(\vec{p}) = (\vec{p}^T U_1 \vec{p} - 1)^2 = 0 \\ Unit_2(\vec{p}) = (\vec{p}^T U_2 \vec{p} - 1)^2 = 0 \\ Unit_3(\vec{p}) = (\vec{p}^T U_3 \vec{p} - 1)^2 = 0 \end{aligned}$$

where U_1, U_2 and U_3 are diagonal matrices defined by

$$U_1 = \begin{cases} U_1(i,i) = 1 & \text{for } i = 1..3 \\ U_1(i,i) = 0 & \text{otherwise} \end{cases}$$

$$U_2 = \begin{cases} U_2(i,i) = 1 & \text{for } i = 5..7 \\ U_2(i,i) = 0 & \text{otherwise} \end{cases}$$

```
SURFACES
PLANE   S1   "S1.dat"
PLANE   S2   "S2.dat"
PLANE   S3   "S3.dat"
END_SURFACES

CONSTRAINTS
ORIENTATION_PLANE_PLANE
S1   S2   120   10e-4
S1   S3   90    10e-4
S2   S3   90    10e-4
END_ORIENTATION_PLANE_PLANE

END_CONSTRAINTS
```

Figure 9. Input file of the tetrahedron object.

$$U_3 = \begin{cases} U_3(i,i) = 1 & \text{for } i = 9..11 \\ U_3(i,i) = 0 & \text{otherwise} \end{cases}$$

The expression of the optimization function is then

$$\vec{p}^T \mathcal{H} \vec{p} + \sum_{l=1}^{3} \lambda_{unit}^{l} Unit_l(\vec{p}) + \sum_{l=1}^{3} \lambda_{angle}^{l} Angle_l(\vec{p})$$

The input file related to this object is shown in Figure 9

7. Experiments

The experiments were carried out on real parts having planar and quadric surfaces (cylinder, cone, sphere). The process of extracting the different surfaces of a given part (Fig.10) starts by scanning the part by a 3D triangulation range sensor. The range measurements are segmented into point sets associated with surfaces by means of the *rangeseg* program [6]. In most of the experiments the range data was collected and registered from different views. Thus, the data is additionally corrupted by the registration error. The degree of corruption is expected to be important since the registration has been achieved manually. Actually we have intentionally performed the registration by hand to check the sensitivity of the algorithm with respect to the registration error.

The section will present two experiments carried out on two multi-quadric objects. These experiments check the behaviour and the experiments of the algorithm as well as the the impact of constraint satisfaction on the quality of object shape reconstruction.

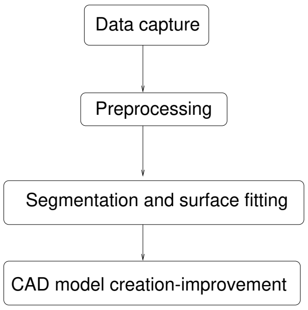

Figure 10. Steps of the object modelling process

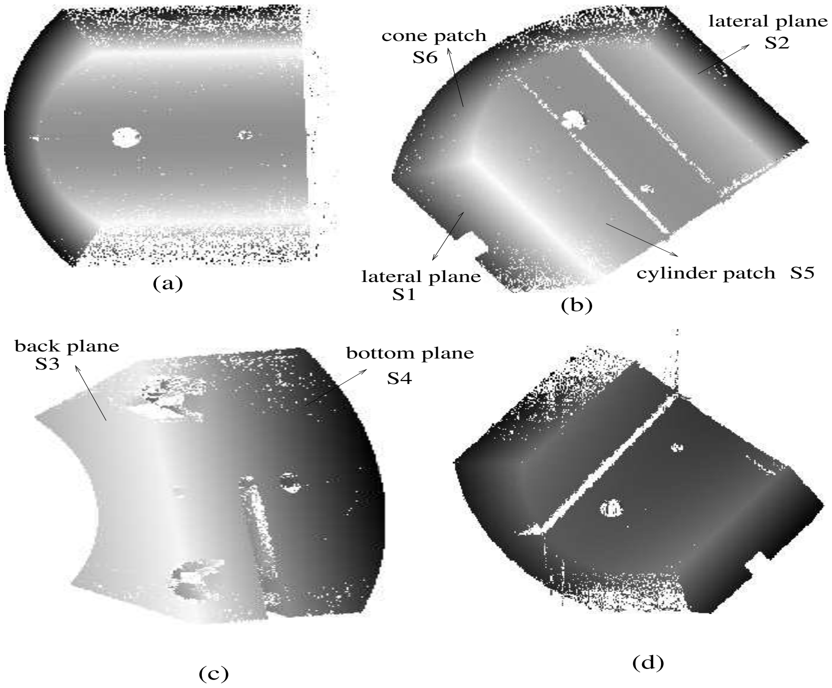

Figure 11. four views of the multi-quadric object

In order to avoid formulas redundancy, the expressions of the different constraints and the way how do they were set up will not be developed. The readers could find more details in [14].

7.1. Reconstruction experiment 1

The object (Fig.11) tested in this experiment comprises two lateral planes S_1 and S_2, a back plane S_3, a bottom plane S_4, a cylindrical surface S_5 and a conic surface S_6. The cylindrical patch is less than a half cylinder (40% arc), the conic patch occupies a small area of the whole cone (less then 30%)

The surfaces of the object have the following constraints:

1. S_1 makes an angle of 120^o with S_2 (we consider the angle between normals).
2. S_1 and S_2 are perpendicular to S_3.
3. S_1 and S_2 make an angle of 120^o with S_4.
4. S_3 is perpendicular to S_4.
5. The axis of the cylindrical patch S_5 is parallel to S_3's normal.
6. The axis of the cone patch S_6 is parallel to S_4's normal.
7. The cylindrical patch is circular.
8. The cone patch is circular.

Constraints 5 and 6 are imposed by associating the normals to S_3 and S_4 respectively to the orientation vectors of the cylinder axis and the cone axis and thus could be combined with the angle constraints (see [14] for explicit development).

The complete optimisation function is then given by the expression:

$$E(\vec{p}) = \vec{p}^T H \vec{p} + \lambda_1 C_{unit}(\vec{p}) + \lambda_2 C_{ang}(\vec{p}) + \lambda_3 C_{circ_{cyl}}(\vec{p}) + \lambda_4 C_{circ_{cone}}(\vec{p})$$

Since the surfaces cannot be recovered from a single view, four views (Fig.11) have been registered by hand. 100 estimations were carried out. At each trial 50% of the surface's points are selected randomly. The results shown in this section are the average of these estimations. The results regarding the algorithm convergence are shown in Figure 12. The behaviour of the different constraints during the optimization have been mapped as a function of the associated λ_i as well as the least squares residual and the sum of the constraint functions. The figures show a nearly linear logarithmic decrease of the constraints. It is also noticed that at the end of the optimization all the constraints are highly satisfied. The least squares error converges to a stable value and the constraint function vanishes at the end of the optimization. This leads to say that the final part shape satisfies the shape constraints at a slight increase in the least squares fitting error. The figures also show that it is possible to continue the optimization further until a higher tolerance is reached, however this is limited practically by the numerical accuracy of the machine. We have noticed that beyond certain values of λ_i some numerical instabilities occurred. This is due as explained in [8] to fact that as long as λ_i become too large the Hessian matrix (involved in the levenberg-Marquardt algorithm) of the optimization function 2 becomes ill-conditioned.

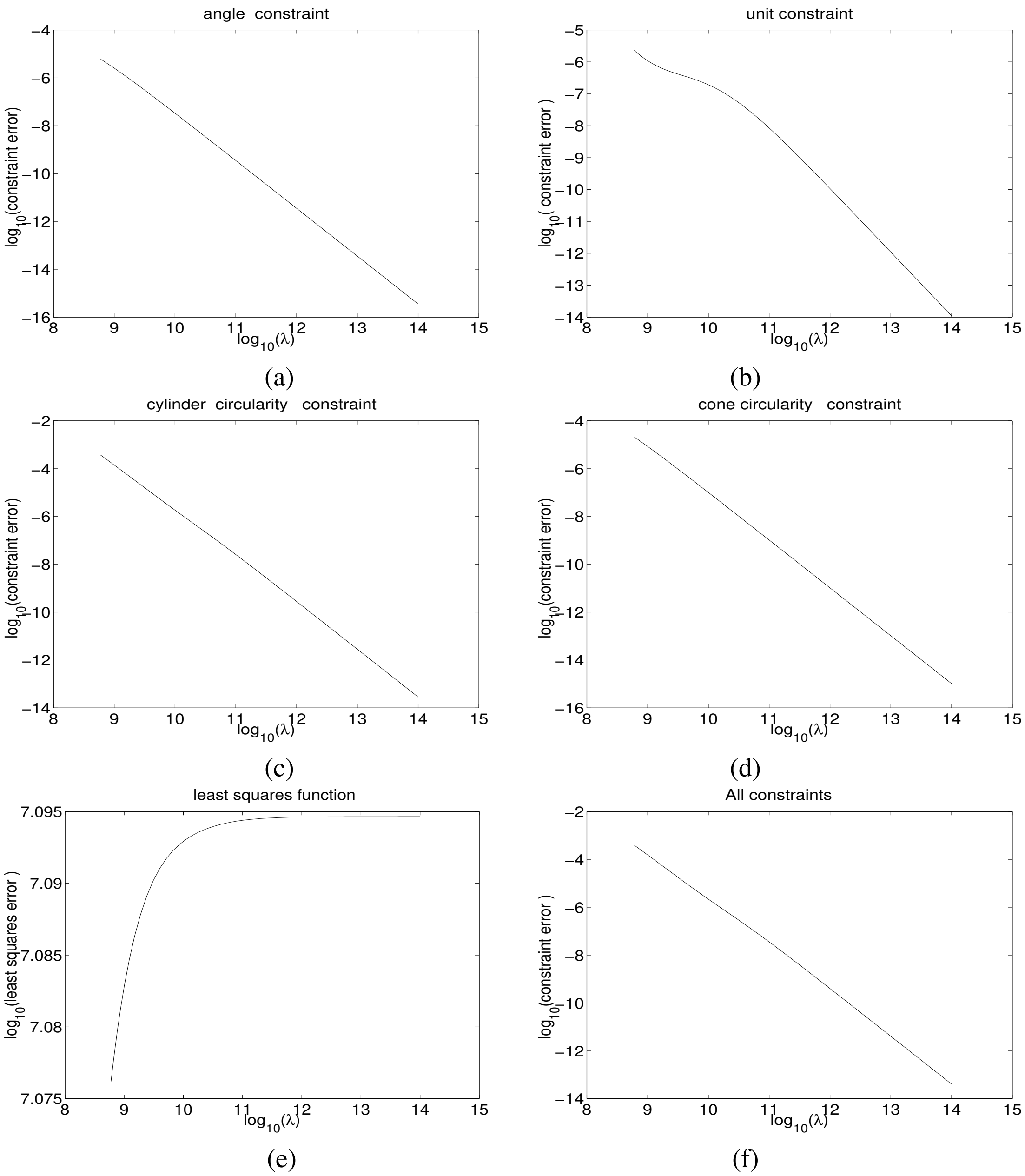

Figure 12. a,b,c,d : Decrease of the different constraint errors as function of the related λ. e,f : Variation of least squares error and the total constraint error.

The angles between the different fitted planes are presented in Table II. It should be noticed that all the angles converge to the actual values. Table III and Table IV contain the estimated values of some attributes of the cylinder and the cone. The values show that each of the axis constraints are perfectly satisfied, the estimated radius and the cone half angle α improve when the constraints are introduced.

Table II. The surface's relative angle estimation with and without constraints.

angle	(S_1, S_2)	(S_1, S_3)	(S_1, S_4)	(S_2, S_3)	(S_2, S_4)	(S_3, S_4)
without constraints	119.76	92.08	121.01	87.45	119.20	90.39
with constraints	120.00^* [1]	90.00^*	120.00^*	90.00^*	120.00^*	90.00^*
actual values	120	90	120	90	120	90

We notice the good shape improvement, relative to the unconstrained least squares method, given by a reduction of bias of about $12mm$ and 3^0 respectively in the radius and the half angle estimation. The standard deviation of the estimations have been reduced as well.

The radius estimation is within the hoped tolerances, a systematic error of about $0.5mm$ is quite nice. However the cone half angle estimation involves a larger systematic error (about 1.8^o). Two factors may contribute to this. The registration error may be too large since the registration was done by hand and the limited area of the cone patch which covers less then 30 % of the whole cone. It is known that when a quadric patch does not contain enough information concerning the curvature, the estimation is very biased, even when robust techniques are applied, because it is not possible to predict the variation of the surface curvature

Table III. The cylinder characteristic estimates with and without constraints.

cylinder parameters	angle(axis, S_3's normal)	radius	standard deviation of radius
without constraints	2.34	37.81	0.63
with constraints	0.00^*	59.65	0.08
actual values	0	60	0

[1] * means that the estimated value is constrained to be equal to the true value.

Table IV. The cone characteristic estimates with and without constraints.

cone attributes	angle(axis, S_4's normal)	α	standard deviation of α
without constraints	6.08	26.01	0.30
with constraints	0.00*	31.83	0.13
actual values	0	30	0

7.2. Reconstruction experiment 2

The object (Fig.13) contains six plane surfaces $S_1, S_2, S_3, S_4, S_5, S_6$, a cylindrical surface S_7 and a spherical surface S_8. The surfaces S_1, S_2, S_3, S_4, S_5 form a square prism, the surface S_5 is a square plane surface.

The cylindrical patch is a whole cylinder and the spherical patch occupies a half sphere.

The surfaces of the object have the following relationships:

1. S_1, S_3 are parallel.
2. S_2, S_4 are parallel.
3. S_5, S_6 are parallel.
4. S_1, S_3 are orthogonal to S_2, S_4.
5. S_5, S_6 are orthogonal to S_1, S_3 and S_2, S_4.
6. S_1, S_3 and S_2, S_4 are separated by the same distance.
7. The cylinder axis is parallel to S_1, S_2, S_3 and S_4 and orthogonal to S_5, S_6.
8. The cylinder axis is located midway between S_1 and S_3 and midway between S_2 and S_4.
9. The cylindrical patch is circular.
10. The sphere centre lies on the cylinder axis.
11. The radius of the cylinder is equal to the radius of sphere.
12. The length diagonal of surface S_5 is equal to the cylinder diameter.

The constraints $1, 2$ and 3 allows a single normal to be associated with each of the pair of planes (S_1, S_3), (S_2, S_4) and (S_5, S_6). The constraint 7 is imposed by associating S_5's normal to to the orientation vector to the cylinder and thus combined with the angle constraints. The other constraints are explicitly defined.

The optimization function is expressed by:

$$E(\vec{p}) = \vec{p}^T H \vec{p} + \lambda_1 C_{unit}(\vec{p}) + \lambda_2 C_{angl}(\vec{p}) + \lambda_3 C_{dist}(\vec{p}) + \lambda_4 C_{axe\_pos}(\vec{p}) \\ + \lambda_5 C_{circ}(\vec{p}) + \lambda_6 C_{sph_{center}}(\vec{p}) + \lambda_7 C_{equ_{radius}}(\vec{p}) + \lambda_8 C_{median}(\vec{p})$$

The surfaces of the objects were recovered from 4 views shown in Figure

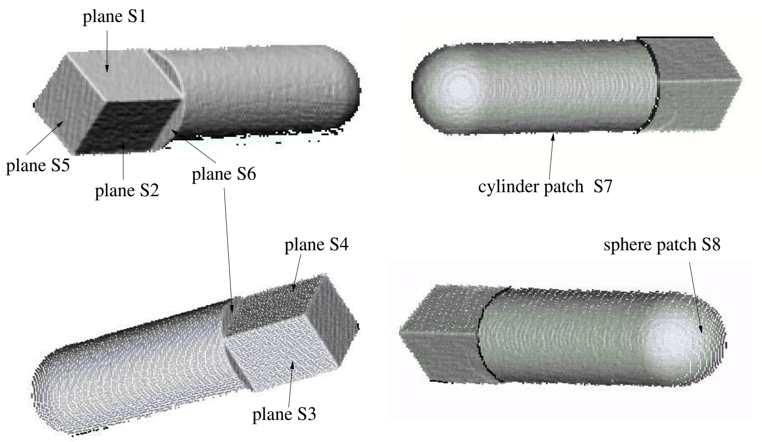

Figure 13. Four views of the multi-quadric object.

13. Similarly to the previous object 100 trials were performed. At each of them 50% of the surfaces's points are selected randomly leading to a different initialisation each trial. In all the trials, the decrease of all the constraint errors and the high level of satisfaction of the constraints at the end of the optimization for a slight increase of the least squares error are essentially similar to that observed in the previous experiments and so similar graphs are not shown here.

7.3. ALGORITHM EVALUATION EXPERIMENTS

Other experiments trials were carried out in order to give answers to the following questions:
1. How stable is the convergence of the algorithm ?
2. How close is the estimation to the actual optimal value ?
3. What are the effects of leaving some features unconstrained ?
4. What is the effect of constraint invalidity ?
5. What is the effect of constraint inconsistency ? 6. Does the global shape improve with local constraints

7.3.1. *Stability of the convergence*

The different estimations resulting from the 100 trials were examined statistically. Figure 14.a shows the maximum and the minimum value (scaled by the absolute value of the mean) for each parameter. The closeness of each pair of extrema is well noticed. This aspect is further confirmed by the standard deviations of the parameters illustrated in Figure 14.b. The distribution of the least squares errors of the different estimations is shown in Figure 15. The related relative variance is 1.94%. Thus we can conclude that the algorithm is stable.

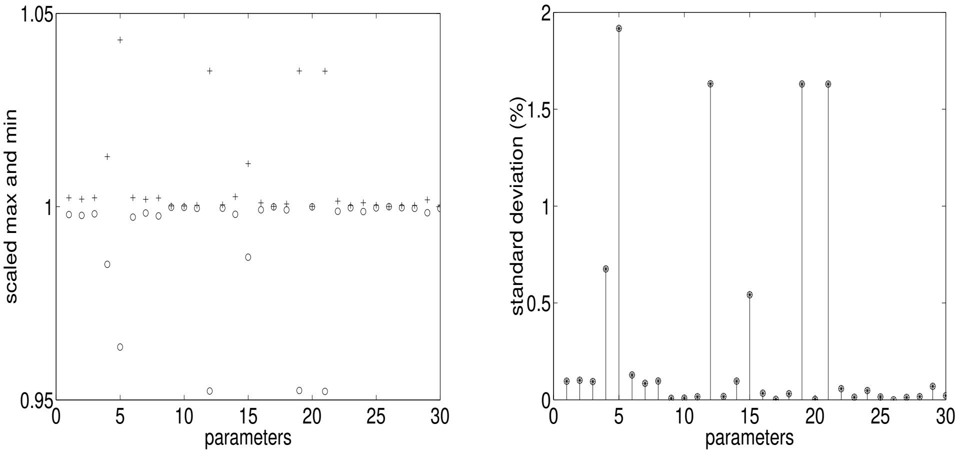

(a) (b)

Figure 14. (a): maximum (+) and minimum (o) value for each parameter scaled by the absolute value of the mean. (b): relative standard deviation of the parameters.

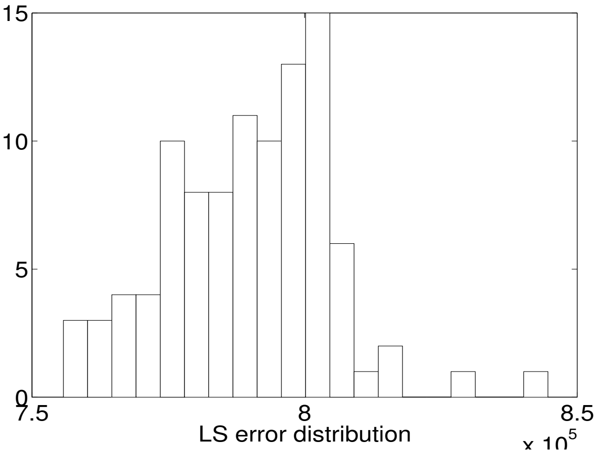

Figure 15. distribution of the least squares errors.

7.3.2. *Closeness to the actual optimal solution*

By "actual optimal solution" we mean the estimation obtained from a process where the constraints are defined, incorporated and satisfied within the least squares error formulation. The solution provided in this case completely satisfies the constraints. So one may ask how close is the estimate obtained by our approach to this optimal solution. As we have mentioned previously, such an ideal and elegant formulation is difficult or impossible to achieve for many objects due to the complexity and to the non-linearity of the geometric constraints. In fact one purpose and motivation of our approach is to overcome this problem. Nevertheless it is possible for some simple particular cases to combine the constraints with the least squares error.

So, in order to make a comparison with the optimal solution a sub-part of the multi-quadric object shown in Figure 13 was considered. It is composed of the two parallel planes S_1 and S_3. The objective is to estimate the planes' orientation taking into account the parallel constraints. For the first case, the parallel constraint is implicitly considered by associating one normal to both planes. The optimization function is then:

$$\vec{n}^T H \vec{n} + \lambda(1 - \vec{n}^T \vec{n})$$

where H is the appropriate data matrix. The second term of the function is the unit constraint. A closed form solution is provided by the eigenvalue method.

In the second case each plane was assigned a different normal vector. The equality of the two normals has to be satisfied through the optimization process. According to our approach the objective function is:

$$\vec{n}_1{}^T H_1 \vec{n}_1 + \vec{n}_3{}^T H_3 \vec{n}_3 + \lambda_1(1 - \vec{n}_1{}^T \vec{n}_1)^2 + \lambda_2(1 - \vec{n}_3{}^T \vec{n}_3)^2 + \lambda_3(1 - \vec{n}_1{}^T \vec{n}_3)^2$$

100 tests were applied for each of the two cases. The average of the results are summarized in Table V. The estimations are similar in the two

Table V. mean estimates of S1 and S3 normal and LS error in the two type of solutions.

	$\vec{n}$	$\vec{n}_1$	$\vec{n}_3$	angle($\vec{n}_1, \vec{n}_3$) (degree)	LS error
1^{st} case	0.5316 0.6733 0.5139	-	-	-	9.07
2^{nd} case	-	0.5316 0.6733 0.5139	0.5316 0.6733 0.5139	0.00	9.06

cases. This shows that both solutions converge to the same value and almost equally minimize the least squares error. The LS of the second solution is slightly lower than the optimal solution one. This is because in the optimal case the constraint is perfectly satisfied so the least squares error has to absorb all the error. The same convergence of the two solutions is further confirmed from the distribution of the difference between the two approaches (angle $(\vec{n},\vec{n}_c)$ where $\vec{n}_c$ is the mean of $\vec{n}_1$ and $\vec{n}_3$) and the difference between the related LS residuals from the 100 trials (Fig.16). Thus we conclude that our optimization process leads us to solution that are very close to the optimal.

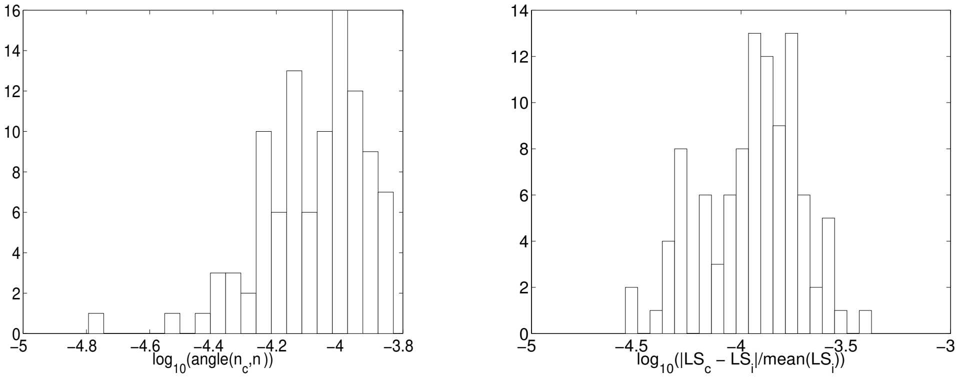

(a) (b)

Figure 16. (a): distribution of the estimation difference. (b): distribution of the LS residuals difference.

7.3.3. *Leaving some features unconstrained*

Another series of tests has been performed without considering the median constraint (constraint 12). This is in order to check if this will affect the position of the four plane surfaces with respect to the cylinder axis and therefore the estimation of the edge of the square surface S_5. Results are shown in Table VI with the previous results for comparison. It is noticed that the radius estimation is not affected but the incorporation of the additional constraints slightly reduces the diagonal length error.

7.3.4. *Invalidity of the constraints*

Suppose that one or more constraints do not reflect the actual relationships between features and therefore are invalid. What would be the behaviour of the algorithm? Will these "false constraints" be satisfied? What could be the resulting estimated model ?

To answer these questions, some angle constraints was set to an incorrect values. Three tests was carried out, in the first the angle $(\vec{n}_1,\vec{n}_2)$ was set to $\pi/3$, in the second the angle $(\vec{n}_1,\vec{n}_5)$ was set to $\pi/3$ and in the third test both

Table VI. comparison of the estimation without median constraints with previous results.

	distance(S_1, S_3)	distance(S_2, S_4)	diagonal of S_5	cylinder radius
without constraints	–	–	–	14.64
with all constraints	21.17	21.17	29.94	14.97
without median constraint	21.15	21.15	29.91	14.97
actual values	21.28	21.28	30.02	15.01

angles $(\vec{n}_1, \vec{n}_5)$ and $(\vec{n}_2, \vec{n}_5)$ were set to $\pi/3$ (note that the correct angles are $\pi/2$ for both angles).

In all these tests the behaviour and the convergence of the algorithm were qualitatively similar to those of the previous experiments. The algorithm converges, the least squares error stabilizes and all the constraints are satisfied at the end of the process although the least squares error is greater than the valid constraints case (Figure 17). Table VII summarizes the estimated model characteristics in each of the three tests.

Table VII. The object characteristic estimates for invalid constraints and true constraints (last row).

	$\vec{n}_1$	$\vec{n}_2$	$\vec{n}_5$	R_{cyl}	R_{sph}	axe_{cyl}	$Center_{sph}$
$(\vec{n}_1, \vec{n}_2) = \pi/3$	-0.61 -0.47 -0.62	-0.58 0.52 -0.62	0.72 -0.02 -0.69	14.97	14.97	0.72 -0.02 -0.69	86.30 -87.38 17.44
$(\vec{n}_1, \vec{n}_5) = \pi/3$	-0.08 -0.60 -0.78	-0.46 0.72 -0.50	0.72 -0.02 -0.69	14.97	14.97	0.72 -0.02 -0.69	86.31 -87.41 17.44
$(\vec{n}_1, \vec{n}_5) = \pi/3$ $(\vec{n}_2, \vec{n}_5) = \pi/3$	-0.02 -0.68 -0.72	0.05 0.72 -0.68	0.72 -0.02 -0.69	14.97	14.97	0.72 -0.02 -0.69	86.31 -87.42 17.44
true constraints	-0.52 -0.67 -0.51	-0.45 0.73 -0.50	0.72 -0.02 -0.69	14.97	14.97	0.72 -0.02 -0.69	86.30 -87.38 17.44

An Examination of Table VII leads to the following observations:
1. In all of the three tests the cylinder and the sphere characteristics are not affected by the invalid constraints.
2. The normal $\vec{n}_1$ which is involved in each of the invalid constraints is affected in three tests.
3. The normal $\vec{n}_2$ is changed in the first and third test where it is involved in the invalid constraints whereas it is unchanged in the second test where it is not involved.

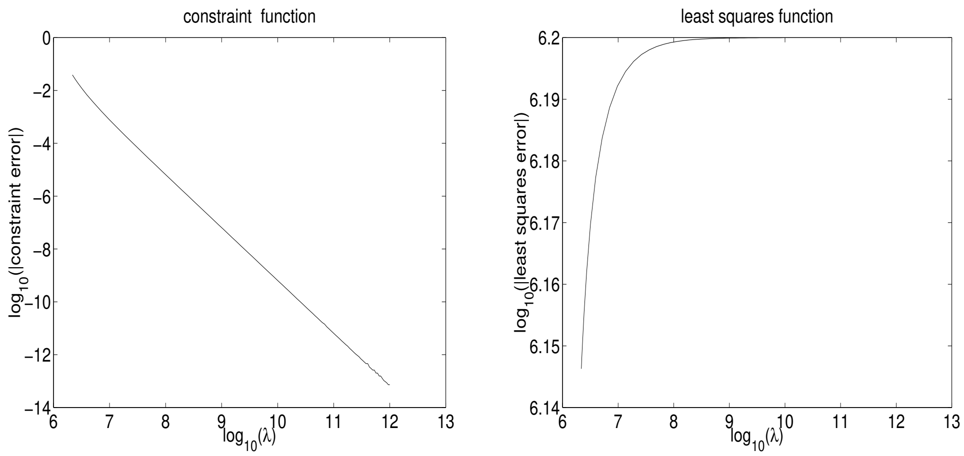

(a)

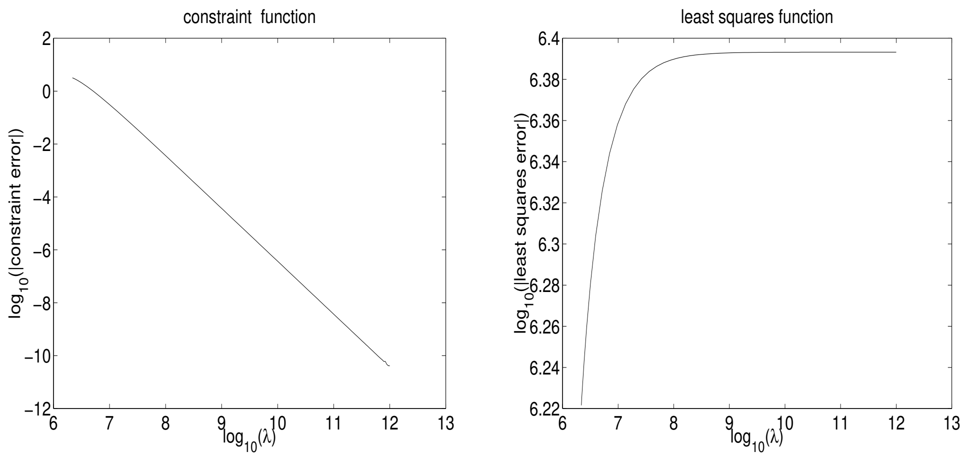

(b)

Figure 17. (a):Constraint error function and least squares error function function for valid constraints. (b):Constraint error and least squares error function for invalid constraints (3^{rd} test).)

4. the normal $\vec{n}_5$ is kept unchanged in all the tests even in those where it is involved in the inconsistent constraints.

From these observations we can deduce that invalid constraints affects the object feature's locations by shifting the involved features toward positions where the invalid constraints are satisfied. Consequently, this will increase the least squares error. The locations and the characteristics of the surfaces which are not involved in the invalid constraints are not affected (the sphere and the cylinder). However the normal $\vec{n}_5$ seems not to satisfy this rule since its orientation stays unchanged for all the cases where it is involved in an invalid constraint. This is explained by the fact that contrary to $\vec{n}_1$ and $\vec{n}_2$,

$\vec{n}_5$ is also involved in other constraints, in particular it is constrained to have the same orientation as the cylinder axis. The satisfaction of this constraint keeps it collinear to the cylinder axis and prevents its orientation from being affected. Thus the algorithm satisfies the invalid constraints in which $\vec{n}_5$ is involved by acting on the other normals involved in these constraints.

7.3.5. *Inconsistency of the constraints*

In this test we investigated what would be the behaviour of the algorithm when some constraints are inconsistent and have a contradiction between them. For this purpose we introduced two additional inconsistent angle constraints (imposing the angles $(\vec{n}_1, \vec{n}_2)$ and $(\vec{n}_1, \vec{n}_5)$ to be $\pi/3$) that conflict with the two original consistent constraints (defining each pair of $(\vec{n}_1, \vec{n}_2)$ and $(\vec{n}_1, \vec{n}_5)$ as orthogonal vectors). The trial carried out with these inconsistent constraints revealed that the algorithm converges normally (Figure 18) with both the least squares and the constraint functions stabilizing at the end of the algorithm. From Figure 18.a we notice that the angle constraints are not satisfied. This is obvious because it is not possible to satisfy conflicting constraints simultaneously. the converging values of the constraint function (the sum of all the constraints) Figure 18.b and the angle constraints error are practically equal at the end of the optimization process. This shows that the other consistent constraints are satisfied. This result is quite useful, it means that an inconsistent set of constraints can be detected by observing the convergence of the constraint error rather than its reduction to zero.

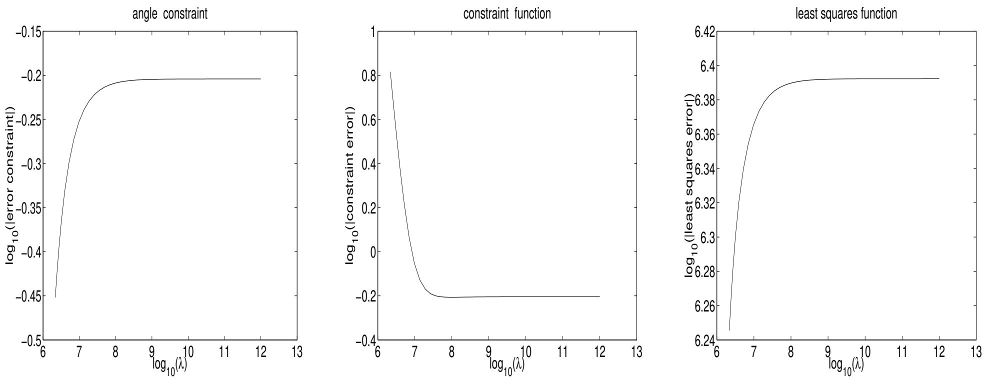

(a) (b) (c)

Figure 18. (a): The sum of the angle constraints' errors. (b): the constraint function. (c) the least squares error

7.3.6. *Global shape improvement*

The different tables shown in this section compare the geometric characteristics of the object for an optimization with and without constraints and show the improvement of the object characteristics estimates when constraints are applied. The results presented in the tables are the average of the 100 estimations. The angles between each pair of surfaces $(S_1, S_2), (S_1, S_5)$ and (S_2, S_5) were set as constraints and the constraints were nearly perfectly satisfied. From Table VIII we notice the satisfaction of the square property of the prism, illustrated by the equality of the two distances separating (S_1, S_3) and (S_2, S_4), their values which is close to the actual length of the edge of the square plane S_5 and closeness of the estimated value of the diagonal of S_5 to the actual value when the constraints are considered. The distances between these last surfaces for an optimization without constraints is not mentioned in this table since the estimated surfaces are not parallel.

Table VIII. Improvement of the prism characteristic estimates.

	distance(S_1, S_3)	distance(S_2, S_4)	diagonal of S_5
with constraints	21.17	21.17	29.95
standard deviation/mean	0.03 %	0.03%	0.03%
actual values	21.28	21.28	30.02

The improvement of the quadric surfaces estimation is confirmed again for this object (Table IX and Table X). The radius estimation error is less than 0.04*mm* for both the cylinder and the sphere. The standard deviations of the cylinder and the sphere radius have been significantly reduced as well.

Table IX. Improvement of the cylinder characteristic estimates.

cylinder parameters	angle(axis, S_5's normal)	radius (mm)
without constraints	1.55	14.64
σ/mean without constraints	-	0.12%
with constraints	0.00*	14.97
σ/mean with constraints	-	0.03%
actual values	0	15.01

Table X. Improvement of the sphere characteristic estimates.

sphere parameters	distance(centre, cylinder axis)	radius (mm)
without constraints	1.36	16.02
σ/mean without constraints	-	0.11%
with constraints	0.00*	14.97
σ/mean with constraints	-	0.03%
actual values	0	15.01

8. Conclusion

This work presents a method for the reconstruction of shape incorporating geometric constraints. It can hold a large number of varied constraint types and incorporates them integrally without the need for linearization.

The experiments carried out on the different objects confirm the convergence of the algorithm. The parameter optimization search does produce shape fitting that satisfies almost perfectly the constraints. They show in particular that the least squares error grows slightly as the constraints are applied and the weighting values increased, but this stabilizes above certain values of the λ_k while the constraint errors are still decreasing. Thus it is possible to satisfy the constraints up to the desired tolerance without seriously affecting the quality of the data fitting. This allows to the user to control the degree of satisfaction of the constraints and to set the tolerances as high as necessary. The processing time for the different objects is typically a few minutes and is is expected to be further reduced with more optimized versions of the implementation.

The above observations suggest that the proposed approach allows flexibility in the incorporation of the constraints, as well as for their satisfaction. Indeed the low computing time of the algorithm allows an interactive user environment. This thing is not possible with techniques requiring several hours computing times such as techniques based on genetic algorithms.

Regarding the slight increases of the LS error, we have to bear in mind that the increase of the least squares residuals value may not reflect a bad estimation in the case when measurement errors are systematic, e.g miscalibration and registration error. This last type of error is expected in our data since the registration process is performed by hand. We believe that the slight increase of the least squares error as a consequence of the constraints satisfaction is a result of the object being located more accurately. However we intend to investigate a more robust form for the objective function involving the data noise statistics.

The different trials applied on the multi-quadric objects confirm the stability of the convergence of the algorithm. The low values of the parameters' variances illustrates the stability of the solution provided by the optimization search process. The tests have shown as well that the proposed approach leads to an estimate which is close to the optimal solution in the case where the constraints could be combined with the least squares error. The experiments also show that applying the constraints to only some features does not seriously affect the estimation of the unconstrained surfaces. The estimation is still improved compared to the case of unconstrained optimization.

The examination of some constraint invalidity cases has shown the constraints are always satisfied whether they are valid or not and the behaviour of the algorithm is typically the same. The satisfaction of an invalid constraints leads to the relocation of the involved and less constrained features (having more degree of freedom) toward positions where the inconsistency is removed. However this will result in a false object model. The trial performed with constraint inconsistency case revealed the same behaviour regarding the convergence of the algorithm but the inconsistent constraints are not satisfied at the end of the optimization. This suggests that constraint validity and consistency checking have to be done before starting the optimization process, or at least examination of the constraint error results to determine if a set of inconsistent constraints have been supplied.

Regarding the shape estimation accuracy, the comparison of the object dimension estimates with those from unconstrained fitting confirms that the proposed approach improves the quality of the shape reconstruction to a high degree. For the second-quadric object the radius of the cylinder and the sphere have an estimation error in the range of $0.04mm$, the edge of the square prism has an estimation error around $0.1mm$. The radius of the cylinder patch estimated from the registered half cylinder has an estimation error around $0.01mm$. For a single a view it is less than $0.5mm$. The same range of error is obtained for the radius of the cylinder patch of the first multi-quadric object.

Results for the cone patch are less satisfactory for the first multi-quadric object. This is mainly due to the relatively small area of the conic patch. Actually, we intentionally chose to work with small patches because unconstrained fitting surface techniques fail to give reasonable estimation in this case (see the radius estimation in Table III) even with robust algorithms due to the "poorness" of the information embodied in the patch.

Although the experiments presented in this work were performed on single objects, the proposed approach can hold simultaneously multiple objects. Indeed, generally industrial parts are designed to fit to each other, so geometric relationships between the parts may be considered and the resulting constraints can be incorporated as well in the optimization process.

Another area we are starting to investigate is how one might automatically identify inter-surface relationships that can have a constraint applied. In manufacturing objects, simple angular and spatial relationships are given by design. So, it should be straightforward to define simple Mahalanobis distance tests that hypothesize standard feature relationships, subject to the feature's statistical position distribution. With this analysis, a computer program could propose a variety of constraints that a human could either accept or reject, after which shape reconstruction could occur.

Finally, although this work is mainly intended for object modelling it may be extended to any constrained built environment application, for example the modelling of the different parts of an industrial plant (pipes, reservoirs,etc) needs the consideration of the geometric relationships between these different parts in order that the whole model will be consistent. The same is true as well for modelling different compartments of buildings or cities.

ACKNOWLEDGEMENT

The work presented in this paper was funded by UK EPSRC grant GR /L25110.

References

1. R. Anderl, R Mendegen, *Modelling with constraints: Theoretical foundation and application* CAD, Vol. 28, No 3, pp 155-168 1996
2. R.M.Bolle, D.B.Cooper *On Optimally Combining Pieces of Information, with Application to Estimating 3-D Complex-Object Position from Range Data.* IEEE Trans. PAMI, Vol.8, No.5, pp.619-638, September 1986.
3. J.De Geeter, H.V.Brussel, J.De Schutter, M. Decreton *A Smoothly Constrained Kalman Filter.* IEEE Trans. PAMI pp.1171-1177, No.10, Vol.19, October 1997.
4. Chang-Xue Feng, A. Kusiak, *Constraints-based design of parts.* CAD, Vol 27 No 5 1995 pp 343 -352, 1995
5. A.F. Fitzgibbon, D.W. Eggert, R.B. Fisher. *High-level CAD model acquisition from range images.* CAD, Vol.29, No.4, pp.321-330, 1997
6. A. Hoover, G. Jean-Baptiste, X. Jiang, P. J. Flynn, H. Bunke, D. Goldgof, K. Bowyer, D. Eggert, A. Fitzgibbon, R. Fisher *An Experimental Comparison of Range Segmentation Algorithms.* IEEE Trans. PAMI, Vol.18, No.7, pp.673-689, July 1996.
7. S.L.S. Jacoby, J.S Kowalik, J.T.Pizzo *Iterative Methods for Nonlinear Optimization Problems.* Prentice-Hall, Inc. Englewood Cliffs, New Jersey, 1972.
8. W. Murray *An Algorithm for Constrained Minimization.* Optimization, Ed. R.Fletcher, pp.247-258, Academic press, Londond, 1969
9. J.Porrill *Optimal Combination and Constraints for Geometrical Sensor Data.* International Journal of Robotics Research, Vol.7, No.6, pp.66-78, 1988.
10. A.A.G. Requicha *Reprsentation of Tolerances in Solid Modelling: Issues and Alternative Approaches* Solid Modelling by Computers: from Theory to Applications, J.W.Boyse amd M.S.Pickett, Eds. New York: Plenum, 1984, pp.3-22
11. A.P. Rockwood, J. Winget. *Three-dimensional object reconstruction from two-dimensional images.*
CAD, Vol.29, No.4, pp.279-286, 1997.

12. B.S. Shin, Y.G. Shin. *Fast 3D solid model reconstruction from orthographic views.* CAD, Vol.30, No.1, pp.63-76.
13. T. Varady, R. R. Martin, J. Cox. *Reverse engineering of geometric models, an introduction* CAD, Vol.29, No.24, pp. 255-268, 1997.
14. N.Werghi, R.B.Fisher, A.Ashbrook, C.Robertson *Modelling Objects Having Quadric Surfaces Incorporating Geometric Constraint.* Proc. ECCV'98, pp.185-201, Freiburg, Germany, June 1998.
15. Q.W. Yan, C.L.P. Chen, Z. Tang. *Reconstruction of 3D objects from orthographic projections.* CAD, Vol.26, No.9, 1994.